ORIGINAL RESEARCH ARTICLE

Optimization of Deposition Conditions of SrZrS$_3$ Perovskite Thin Films Grown by Chemical Bath Deposition

Areej Fatima[1] · Shahid Iqbal[2] · Tanzeela Fazal[3] · Bushra Ismail[1] · Mazloom Shah[4] · Ambreen Ayub[5] · Qaiser Mahmood[6] · Nasser S. Awwad[7] · Hala A. Ibrahium[8] · Foziah F. Al-Fawzan[9] · Eslam B. Elkaeed[10]

Abstract

Chalcogenide perovskites are receiving considerable attention as a new type of semiconducting material for optoelectronic applications. The current work is carried out on optimization studies for depositing SrZrS$_3$ perovskite thin films via chemical bath deposition. The film properties were investigated as a function of molar concentration ratios (0.4–0.6 M), complexing agent, pH (9–10), deposition time (14–20 h), and annealing temperature (300–500°C). The orthorhombic structure of the deposited thin film was verified by x-ray diffraction (XRD) investigation. The Pnma space group was identified by XRD investigations with lattice constants of 7.09 Å, 9.77 Å, and 6.78 Å. The optical characteristics of the films were examined using a UV–Vis spectrophotometer. Bandgap values in the range of 3.34–3.50 eV, and absorption coefficient 1.75×10^4 cm^{-1} to 2.15×10^4 cm^{-1} were observed for the synthesized samples. It was found that 500°C for the annealing temperature and a pH of 10 were the optimal values for the SrZrS$_3$ thin film deposition parameters.

Areej Fatima and Tanzeela Fazal have equally contributed to this work.

✉ Shahid Iqbal
shahidiqbal@hzu.edu.cn

✉ Bushra Ismail
bushraismail@cuiatd.edu.pk

1 Department of Chemistry, COMSATS University Islamabad (CUI), Abbottabad Campus, Abbottabad 22010, Pakistan

2 Nottingham Ningbo China Beacons of Excellence Research and Innovation Institute, University of Nottingham Ningbo China, Ningbo 315100, People's Republic of China

3 Department of Chemistry, Abbottabad University of Science and Technology (AUST), Abbottabad, Pakistan

4 Department of Chemistry, Faculty of Science, Grand Asian University Sialkot, Sialkot, Pakistan

5 Department of Physics, Women University of Swabi, Swabi, Pakistan

6 Chemistry and Chemical Engineering Guangdong Laboratory, Shantou 515031, People's Republic of China

7 Chemistry Department, Faculty of Science, King Khalid University, P.O. Box 9004, 61413 Abha, Saudi Arabia

8 Biology Department, Faculty of Science, King Khalid University, P.O. Box 9004, 61413 Abha, Saudi Arabia

9 Department of Chemistry, College of Science, Princess Nourah bint Abdulrahman University, P.O. Box 84428, 11671 Riyadh, Saudi Arabia

10 Department of Pharmaceutical Sciences, College of Pharmacy, AlMaarefa University, 13713 Riyadh, Saudi Arabia

Introduction

Crystalline silicon is currently dominating the photovoltaics (PV) industry due to its high efficiency.[1] A single-junction c-Si PV cell's theoretical maximum power conversion efficiency is roughly 29%, which can be increased to 43% by stacking a second p–n junction.[2–4] The development

of lead halide perovskite, an emerging material with an efficiency of around 30%, has facilitated the construction of more affordable solar cell absorbers.[5,6] For mass manufacturing, conventional perovskite presents two major challenges. The first issue with lead halide perovskites is their intrinsic chemical instability, and the second is that lead is one of their hazardous constituents.[7,8] To address

these issues, it has been shown that non-halide perovskites with numerous constituents are an acceptable substitute. In particular, chalcogen halides have received considerable attention in this area because of their notable chemical stability in the air up to 400°C, which has been shown experimentally, and their optoelectronic properties with absorption coefficient values of more than 105 cm^{-1}.[9–11]

Table I Composition of bath solutions for SrZrS$_3$ perovskite thin film optimization.

No.	Sample	Bath composition	Complexing agent	pH	Annealing temperature
1	A1	Sr precursor = 0.40 M Sr(NO$_3$)$_2$ Zr precursor = 0.60 M ZrOCl$_2$.8H$_2$O S precursor = 1.16 M CH$_3$CSNH$_2$ Solvent = 20 ml H$_2$O	No	9	No
2	A2	Sr precursor = 0.60 M Sr(NO$_3$)$_2$ Zr precursor = 0.90 M ZrOCl$_2$.8H$_2$O S precursor = 5.80 M CH$_3$CSNH$_2$ Solvent = 20 ml H$_2$O	No	9	No
3	A3	Sr precursor = 0.60 M Sr(NO$_3$)$_2$ Zr precursor = 0.90 M ZrOCl$_2$.8H$_2$O S precursor = 5.80 M CH$_3$CSNH$_2$ Solvent = 20 ml H$_2$O	0.1 M C$_{10}$H$_{16}$N$_2$O$_8$	9	No
4	A4	Sr precursor = 0.60 M Sr(NO$_3$)$_2$ Zr precursor = 0.90 M ZrOCl$_2$.8H$_2$O S precursor = 5.80 M CH$_3$CSNH$_2$ Solvent = 20 ml H$_2$O	0.1 M C$_{10}$H$_{16}$N$_2$O$_8$	10	No
5	A5	Sr precursor = 0.60 M Sr(NO$_3$)$_2$ Zr precursor = 0.90 M ZrOCl$_2$.8H$_2$O S precursor = 5.80 M CH$_3$CSNH$_2$ Solvent = 20 ml H$_2$O	0.1 M C$_{10}$H$_{16}$N$_2$O$_8$	10	300°C
6	A6	Sr precursor = 0.60 M Sr(NO$_3$)$_2$ Zr precursor = 0.90 M ZrOCl$_2$.8H$_2$O S precursor = 5.80 M CH$_3$CSNH$_2$ Solvent = 20 ml H$_2$O	0.1 M C$_{10}$H$_{16}$N$_2$O$_8$	10	500°C

$$Sr(NO_3)_2 = Sr^{2+} + 2NO_3^-$$
$$ZrOCl_2 . 8H_2O = ZrO_2 + 2HCl + 7H_2O$$
$$ZrO_2 + 2HCl = Zr^{4+} + H_2O + Cl_2$$
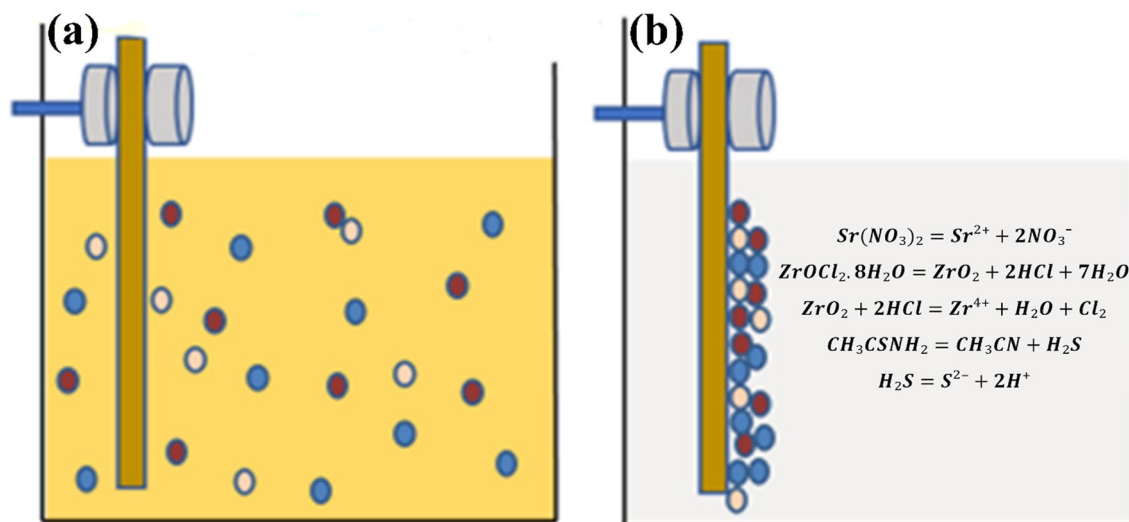$$CH_3CSNH_2 = CH_3CN + H_2S$$
$$H_2S = S^{2-} + 2H^+$$

Fig. 1 Deposition of SrZrS$_3$ perovskite by CBD (a) at the initial stage and (b) condensation ion-by-ion on substrate.

Numerous chalcogenide perovskites, such as CaZrS$_3$, SrZrS$_3$, SrTiS$_3$, and BaZrS$_3$, have been reported to have a broad adjustable bandgap range of 1.73–2.87 eV.[12] Because of the excellent dielectric response and ferroelectric polarization, strontium zirconium sulfide (SrZrS$_3$) is a notable and reasonably inexpensive perovskite material. SrZrS$_3$ exists in different phases including cubic, orthorhombic, rhombohedral and tetragonal, depending upon the heat treatment. Because of the temperature-dependent phase changes in crystal structure, perovskite materials exhibit distinctive characteristics.[13] However, photovoltaic applications of chalcogenide perovskites are restricted due to the lack of deposition of good-quality thin films. To synthesize perovskite thin films, various scalable deposition processes have recently been set up, such as sol-gel method via dip/spin coating,[14] spray coating,[15] vacuum thermal deposition,[16] soft chemical process,[17] doctor-blading,[18] molecular beam epitaxy,[19] electrodeposition,[20] pulsed laser deposition (PLD),[21] slot-die coating,[22,23] sputtering[24] and chemical bath deposition (CBD).[25]

CBD is one of the simplest chemical processes for thin film deposition.[26] In comparison to alternative deposition techniques, CBD provides many benefits, including large surface area coverage, affordability,[27] reduced material waste, simplicity of procedure[28] and ease of management.[29,30] Molar ratios, solution pH, deposition duration, annealing temperature, and the nature of solvents and precursors are a few variables that impact the thin film's structure and quality. In the chemical bath deposition technique, thin film deposition is achieved via precipitation, which involves controlled chemical reactions, and substrates are dipped in solutions containing chalcogenide ion and metal sources.[31] For the fabrication of SrZrS$_3$ perovskite thin films, a solution containing strontium nitrate, zirconium oxychloride octahydrate, thioacetamide and ethylenediaminetetraacetic acid (EDTA) can be employed. When employing the CBD approach, EDTA mainly functions as a complexing agent for the strontium and zirconium ions in the reaction solution.[32]

The CBD method is used in the current investigation to deposit thin films of SrZrS$_3$perovskite in order to optimize the CBD technique for deposition of SrZrS$_3$ perovskite for commercial silicon solar cells. This paper will help understand the effect of different key influential aspects, including concentration of initial precursor solutions, stoichiometry, and annealing temperature, which regulate the resultant optical properties including bandgap,[33,34] absorption coefficient, dielectric constant,[35] extinction coefficient and refractive index[36] of the deposited films. Investigations have also been done on structural variations of the deposited films.
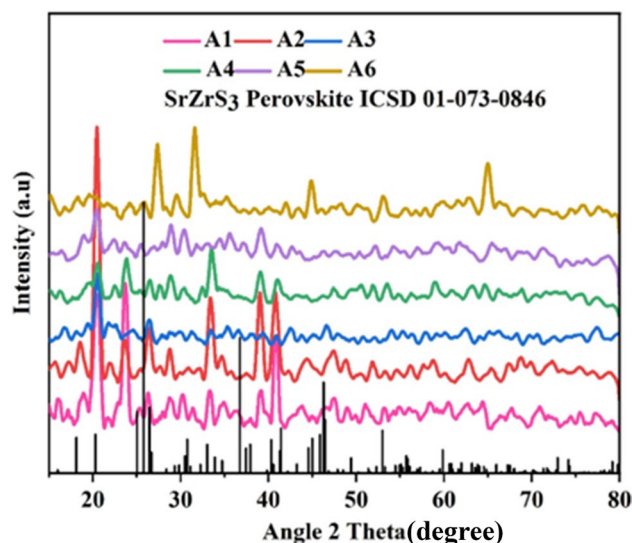

Fig. 2 X-ray diffraction pattern of SrZrS₃ perovskite thin films deposited at different conditions.

Materials and Methods

The following chemicals were used in the current work to synthesize SrZrS$_3$ perovskite thin films: strontium nitrate [Sr(NO$_3$)$_2$, purity 99%, BDH], zirconium oxychloride octahydrate (ZrOCl$_2$.8H$_2$O, purity 93%, Sigma Aldrich), thioacetamide (CH$_3$CSNH$_2$, purity 99%, BDH), ethylenediaminetetraacetic acid (C$_{10}$H$_{16}$N$_2$O$_8$, purity 98.5%, DaeJung), ammonium hydroxide (NH$_4$OH, purity 97%, DaeJung), hydrochloric acid (HCl, purity 37%, BDH), ethanol (CH$_3$CH$_2$OH, purity 99%, DaeJung), nitric acid (HNO$_3$, purity 70%, Sigma Aldrich) and sulfuric acid (H$_2$SO$_4$, purity 97%, DaeJung).

Thin films were created on commercial glass surfaces measuring 75 mm × 25 mm × 1 mm after the solutions were prepared in deionized water. Before air-drying, the substrates underwent a thorough rinsing in acetone for 30 min and double-distilled water for 20 min. First, the substrates were cleaned for 60 min in a diluted sulfuric acid solution (H$_2$SO$_4$/H$_2$O, 1:5, v/v) to get rid of the native oxide layer.[37]

The composition of the bath solutions is shown in Table I. Glass substrates that had been previously cleaned were positioned vertically in the solution at the specified pH and deposition time. Theoretically, thin films grow via an ion-by-ion growth mechanism.[38,39] According to the nominal 1:1:3 (Sr:Zr:S) ratio, the inorganic phase's nuclei develop in a directed manner on the substrate as a result of heterogeneous nucleation.[40] The substrates were removed from the bath

Table II Crystallographic aspects of SrZrS$_3$ perovskite thin films (A1 to A6) deposited at different optimization conditions.

| Samples	Calculated lattice constants			d-Spacing value (Å) 3.45*(121)	Cell volume (Å^3) 467*	Average crystallite size (nm)	X-ray density (g cm^{-3}) 3.91*
	a (Å) 7.11*	b (Å) 9.77*	c (Å) 6.74*				
A1	7.04	9.47	6.65	1.99 (132)	450	32	4.06
A2	7.10	9.55	6.93	3.53 (002)	470	39	3.89
A3	7.01	9.67	6.79	4.22 (111)	459	44	3.98
A4	7.22	9.79	6.79	3.32 (002)	481	50	3.80
A5	7.12	9.78	6.80	2.40 (202)	473	55	3.87
A6	7.09	9.77	6.78	3.43 (121)	470	58	3.89

*ICSD 01-073-0846
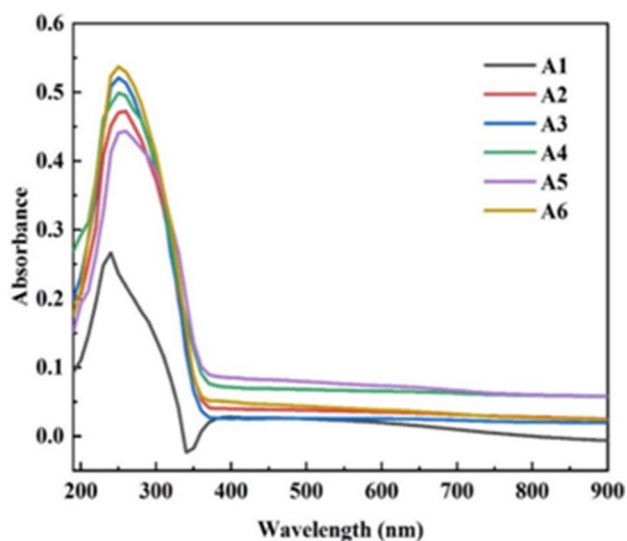
Fig. 3 Variation in absorbance versus wavelength for SrZrS$_3$ perovskite thin films (A1–A6) deposited at different optimization conditions.
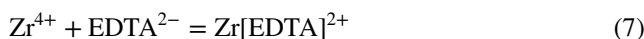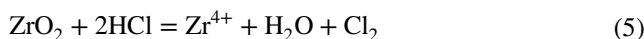
after 6 h of deposition, dried at 40°C, and then stored in a small, airtight container. Deposited SrZrS$_3$ thin films were homogeneous and adhered to the substrates. Additionally, a few thin films were subjected to heat treatment in a muffle furnace for 2 h at 500°C. To assess their optoelectronic behavior, deposited samples were subjected to characterization procedures. X-ray diffraction (XRD; Bruker AXS, Karlsruhe, Germany) was conducted to examine the crystalline structure of the deposited films. The optical absorbance of the films was measured in the 200–900 nm wavelength region using a UV–Vis spectrophotometer (PerkinElmer Lambda 2S).
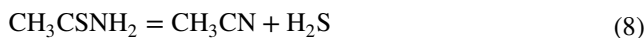
Results and Discussion

Sr^{2+}, Zr^{4+}, and S^{2-} ions were slowly released into solution during the deposition process of SrZrS$_3$ perovskite thin films, which subsequently condensed ion-by-ion on substrates.[41] By dissociating a complex species of Sr[EDTA]$^{2-}$ and Zr[EDTA]$^{2+}$ (complexation occurs at pH 10), which then interacts with sulfur-containing substances available in baths like thioacetamide (Fig. 1), the complexing agent complexes the metal ions to control their release as shown in Eqs. 1–3.

$$Sr(NO_3)_2 = Sr^{2+} + 2NO^{3-} \tag{1}$$

$$EDTA = EDTA^{4-} + 4H^+ \tag{2}$$

$$Sr^{2+} + EDTA^{4-} = Sr[EDTA]^{2-} \tag{3}$$
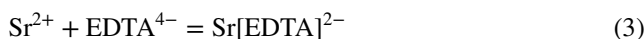
Zirconium oxychloride octahydrate as a source of Zr^{4+} was also made complex with EDTA to control the release of zirconium ions. The following reaction shows the complexing of zirconium with EDTA.
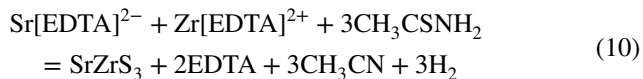
$$ZrOCl_2.8H_2O = ZrO_2 + 2HCl + 7H_2O \tag{4}$$

$$ZrO_2 + 2HCl = Zr^{4+} + H_2O + Cl_2 \tag{5}$$

$$EDTA = EDTA^{2-} + 2H^+ \tag{6}$$

$$Zr^{4+} + EDTA^{2-} = Zr[EDTA]^{2+} \tag{7}$$

The sulfide ions are released in the manner described below:

$$CH_3CSNH_2 = CH_3CN + H_2S \tag{8}$$

$$H_2S = S^{2-} + 2H^+ \tag{9}$$

The overall reaction is as follows:

$$Sr[EDTA]^{2-} + Zr[EDTA]^{2+} + 3CH_3CSNH_2$$
$$= SrZrS_3 + 2EDTA + 3CH_3CN + 3H_2 \tag{10}$$

The reaction sequences clearly show that the HS^- ions will predominate in solution while the S^{2-} ions are maintained at a low concentration. The forward reaction will be made easier in equilibrium if the content of S^{2-} ions is increased by the addition of hydroxide ions.

The XRD patterns of the deposited films are shown in Fig. 2. The films have an orthorhombic single-crystalline structure, according to this diffraction pattern, which is a good match for ICSD #01-073-0846. Sharp peaks in the x-ray diffractogram show the crystalline structure of the material. In most of the deposited samples, an intense peak was observed at 25.765° with the hkl plane (121). Two other prominent peaks were observed at 36.735° and 46.268° with hkl planes (202) and (123), respectively.

The growth mechanism of thin films is typically influenced by the chemistry of precursors, pH, complexing agent and annealing temperature. According to diffraction patterns, A2 (0.6 M) showed higher crystallization as compared to the other concentrations, i.e., 0.4 M (A1). Diffraction peaks confirmed that a more basic medium was suitable for deposition, and in comparison with the bath at pH 9 (A4), crystallinity was higher at pH 10 (A3). With the increase in annealing temperature, crystallinity was also found to be higher.

The crystallite size was found to increase with increasing concentrations of the precursors due to the availability of more ions at higher concentrations (Table II). The crystallite size of the perovskite thin films was increased with the addition of a complexing agent. EDTA was used as a complexing agent. It forms complexes with strontium and zirconium ions, which then slowly release the cations, leading to a gradual increase in ionic product with time. With the increase in pH, more hydroxyl ions were available in the solution, leading to enhanced precipitation and hence good deposition of the films. Increasing the annealing temperature also resulted in an increase in crystallite size from 50 nm to 58 nm. With higher concentrations of the precursors and basicity, ions tend to preferentially occupy the octahedral sites, resulting in shrinkage in the volume of the cell. The volume of the cell also decreases with the addition of a complexing agent, as there are more hydroxyl ions available when EDTA is added to cover the unoccupied sites. The volume of the cell decreases with increasing pH values and annealing temperatures. The x-ray density increases with increasing concentration of precursors and with the addition of complexing agent and pH values as well as with increasing annealing temperature.

Figure 3 shows UV–Vis absorption spectra of SrZrS₃ perovskite at different optimized conditions obtained in the range of 200–900 nm. A wide absorption band between 238 nm and 258 nm and an absorption edge at 360 nm were observed in all films. To determine the bandgap of a deposited film, the Tauc equation is used.[42]

$$(\alpha h\nu)^r = A(h\nu - E_g) \tag{11}$$

where α is the absorption coefficient, h is the Planck constant (6.62×10^{-34} Js), ν is the frequency of light, A is a constant, and E_g is the optical bandgap.

Absorbance (A) and transmittance (T) are directly related to each other:

$$A = -\log(T) \tag{12}$$

R stands for reflectance, which is computed using Eq. 13:

$$R = 1 - [T \exp(A)]^{1/2} \tag{13}$$

The adsorption coefficient is computed using the formula below:

$$\alpha\,(cm^{-1}) = \frac{1}{d} \cdot \frac{\ln(1-R)^2}{T} \tag{14}$$

The refractive index (n) can be calculated by the following formula:

$$n = \left[\frac{4R}{R-1} - k^2\right]^{1/2} - \left[\frac{R+1}{R-1}\right] \tag{15}$$

The wavelength and absorption coefficient values can be used to determine the extinction coefficient (k), as shown in Eq. 16:

$$k = \frac{\alpha\lambda}{4\pi} \tag{16}$$

Another measure derived from UV-Vis absorbance data is the dielectric constant, in which both the refractive index and extinction coefficient play a role[43]:
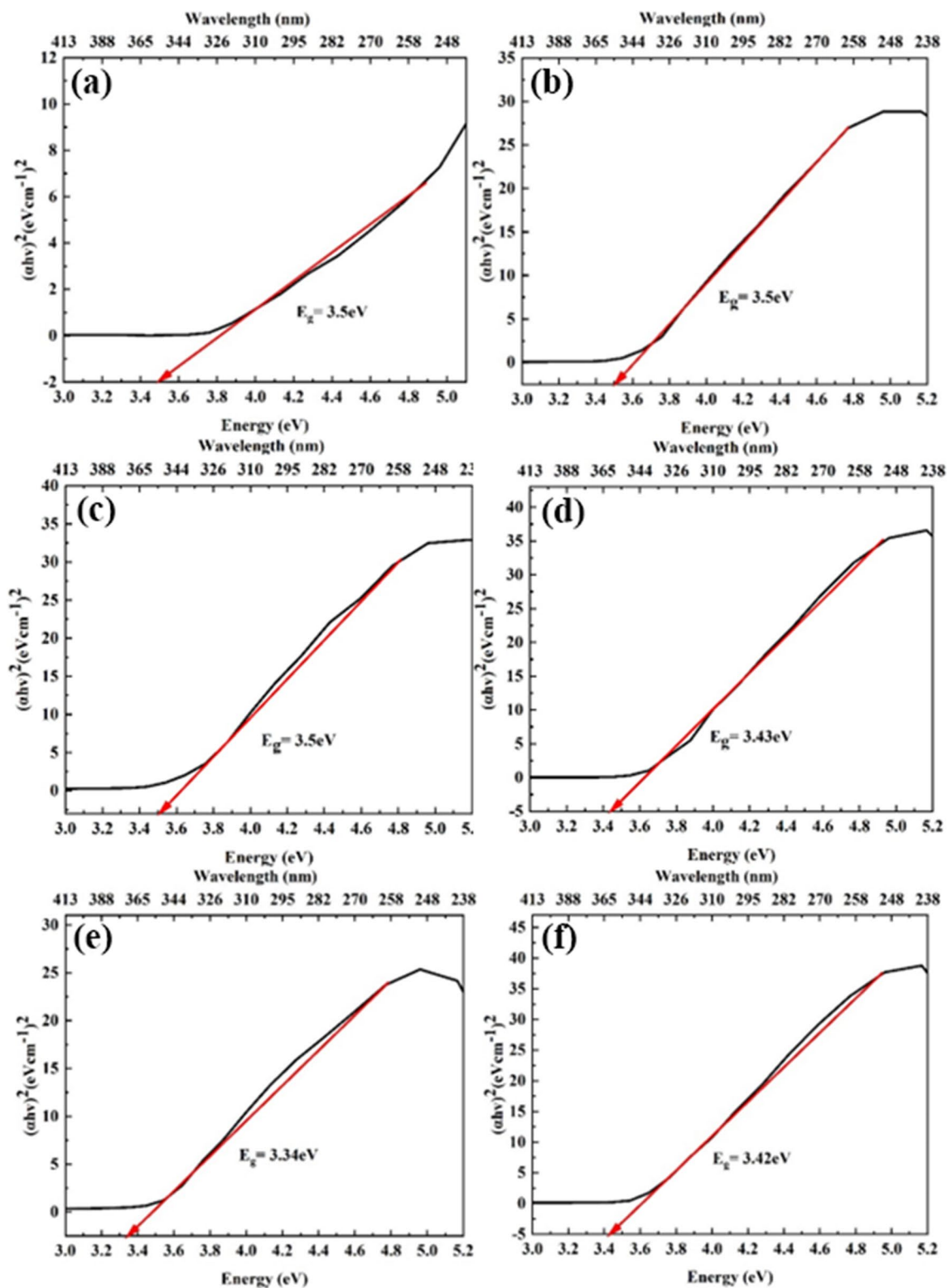
$$\varepsilon = (n - k) \tag{17}$$

Fig. 4 Tauc plots for bandgap of SrZrS$_3$ perovskite thin films (a) to (f) deposited at different optimization conditions.
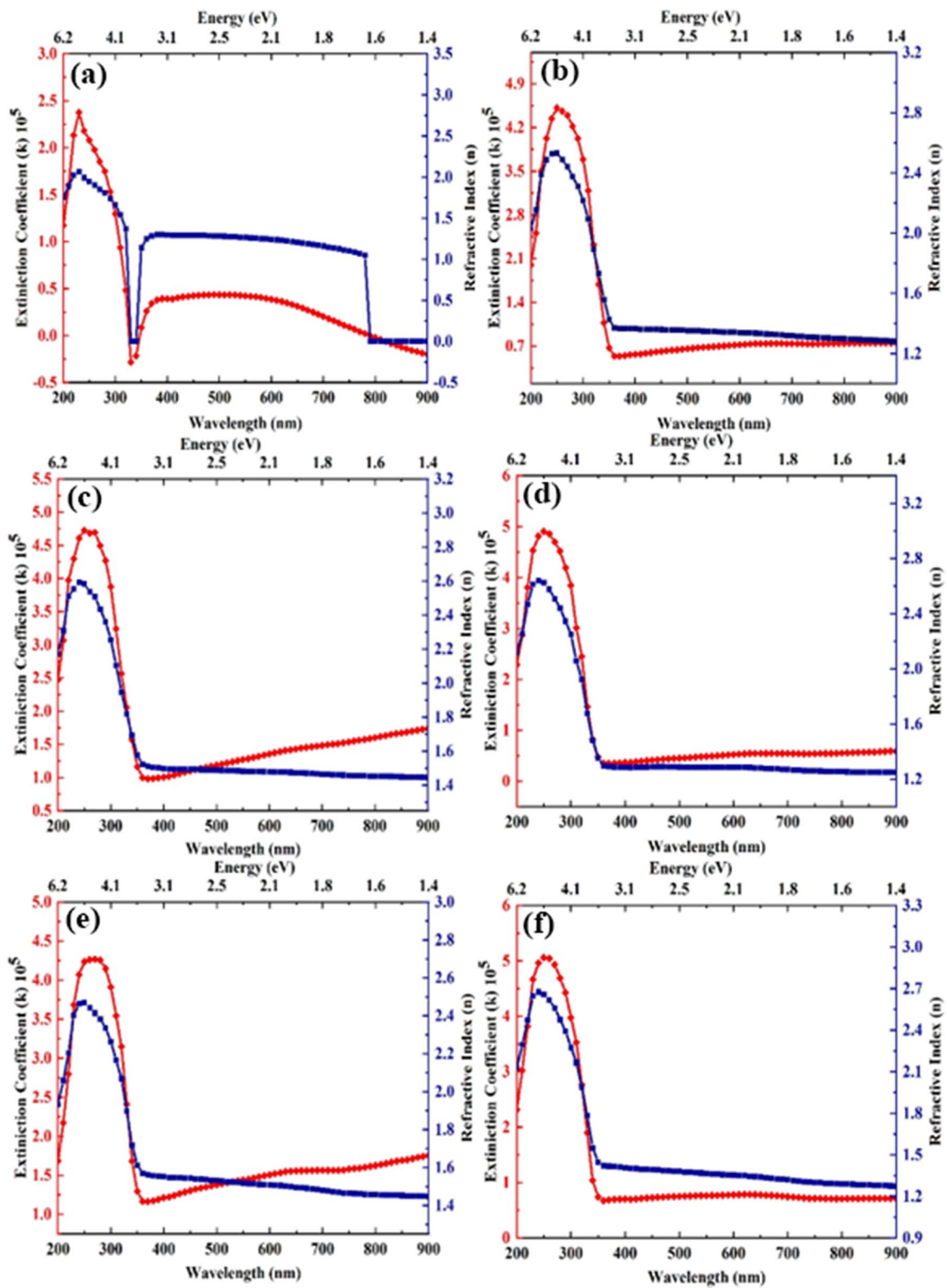
Fig. 5 SrZrS₃ perovskite thin films (a) to (f) deposited under various optimization settings: total excitation coefficient and refractive index.

Electrical conductivity can be calculated mathematically as follows:

$$\sigma_e\left(\Omega\text{cm}^{-1}\right) = \frac{2\pi}{\lambda nc} \qquad (18)$$

Equation 19 determines the optical conductivity[44]:

$$\sigma_0\left(\text{s}^{-1}\right) = \frac{anc}{4\pi} \qquad (19)$$

Thermal conductivity is determined by Eq. 20:

$$\sigma_T\left(\text{Wm}^{-1}\text{K}^{-1}\right) = LT\sigma_e \qquad (20)$$

L is the Lorentz number 2.45×10^{-8} WΩK^{-2}. The optical density of thin film is found by Eq. 21:

$$\text{OD} = \alpha t \qquad (21)$$

In this equation, t is film thickness and α is the absorption coefficient.

All films were found to have reflectance of around 15–30%. The variation in bandgap values for the deposited thin films is attributed to different initial concentrations, complexing agents, pH, and annealing (Figs. 4 and 5).

According to UV-Vis spectroscopy measurements, the bandgap of the films varied from 3.34 eV to 3.50 eV. The crystalline structure of thin films is one factor that affects bandgap values, among many others. From the thin-film absorption studies, the optical parameters, such as the absorption coefficient, penetration depth, extinction coefficient, refractive index, dielectric constants, and electrical, thermal, and optical conductivities, were computed. The absorption coefficient is the optical parameter that influences how much light a material absorbs per thickness. A greater absorption coefficient indicates that the material absorbs more photons per unit thickness. The absorption coefficient is denoted by α. Figure 6 shows the absorption coefficient bar chart of SrZrS$_3$ thin films deposited at different optimization conditions.

The dielectric constant is the ratio of the force between two charges in a space to the force between two charges in a medium. Table III tabulates the values of the dielectric constants of SrZrS$_3$ thin films deposited at different initial concentrations, the effect of complexing agent, the effect of pH, and the effect of annealing temperature. Electrical conductivity is the amount of heat or energy needed to cause an amount of charge to flow. The electrical conductivity of the synthesized SrZrS$_3$ perovskite samples was 3.7 Ω cm^{-1} to 4.6 Ω cm^{-1}. A material's optical conductivity is at its highest when its absorbance is higher. The optical conductivity of optimized SrZrS$_3$ perovskite was 10.4 s^{-1} to 13.7×10^{13} s^{-1}. The ability of a material to conduct or transfer heat is referred to as thermal conductivity, which is determined by the material's structure as well as its composition.

The thermal conductivity of thin film in the presence of the complexing agent is lower than that in the absence of the complexing agent. With the addition of EDTA as a complexing agent, the thermal conductivity of the material decreases due to the presence of free electrons in EDTA, which leads to an increase in the population of molecules, and ultimately increased hindrance is also observed. Thin films with a more basic medium show less thermal conductivity with the addition of NH$_4$OH as a base, which decreases because of the hindrance of free electrons present as OH$^-$ ions. With the
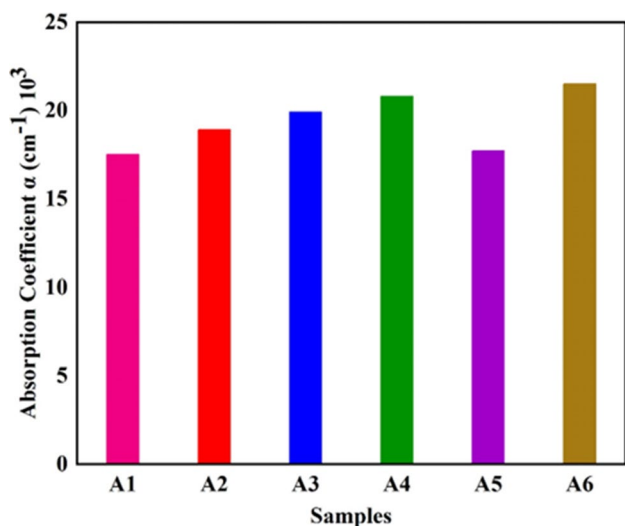

Fig. 6 UV-Vis absorption coefficient spectra of SrZrS$_3$ perovskite thin films (A1 to A6) deposited at different optimization conditions.

Table III Optical properties of SrZrS$_3$ perovskite studied by UV–Vis spectroscopy.

Factors	A1	A2	A3	A4	A5	A6
Absorption coefficient (10^3 cm^{-1})	17.5	18.9	19.9	20.8	17.7	21.5
Penetration depth (10^{-4} cm)	2.0	2.0	3.8	2.9	1.8	3.0
Extinction coefficient (10^5)	4.4	4.5	4.7	4.9	4.2	5.0
Refractive index	2.4	2.5	2.6	2.7	2.4	2.6
Dielectric constant	6.6	6.7	6.9	7.2	6.3	7.4
Electrical conductivity (Ω cm)$^{-1}$	4.6	3.8	4.5	4.2	3.7	4.1
Optical conductivity (10^{13} s^{-1})	10.5	11.4	12.3	13.1	10.4	13.7
Thermal conductivity (10^{-3} W/m k)	3.4	2.8	3.3	2.3	2.2	2.2

annealing of the sample, thermal conductivity was also decreased. The output of the calculation of the absorption coefficient, penetration depth, extinction coefficient, refractive index, dielectric constant, and electrical, optical, and thermal conductivity from optical parameters is shown in Table III. Metals have high optical conductivity and extinction coefficient (k) values, which causes reflectance to be close to unity, but semiconductors have lower values for both, which leads to lower reflectance and higher transparency over metals.

Conclusions

In this study, CBD was used to develop SrZrS3 perovskite thin films at room temperature on glass substrates. The CBD approach is used for the first time to understand the relationships and importance of the factors that affect film quality. The pH and annealing temperature were shown to be the most important parameters in the deposition. The ideal $SrZrS_3$ thin film deposition parameters were pH 10, deposition time of 20 min, and annealing temperature of 500°C. According to the XRD data, deposited films had a crystalline orthorhombic structure. According to the various deposition conditions, the optical bandgap energy values ranged from 3.34 eV to 3.50 eV. Absorption coefficient in the range of 1.75×10^4 cm^{-1} to 2.15×10^4 cm^{-1} was studied for the synthesized samples. Hence, using CBD, and varying the optimization parameters, the performance of the perovskite thin films can be maximized as a scalable printing technique for industrial applications.

Author Contributions The manuscript was written with the contributions of all authors. All authors have approved the final version of the manuscript.

Data availability The datasets generated during and/or analyzed during the current study are available from the corresponding author upon reasonable request.

Conflicts of interest There are no conflicts to declare.

References

1. N. Jaiswal, D. Kumari, R. Shukla, and S.K. Pandey, Design and performance optimization of eco-friendly Cs₂AgBiBr₆ double perovskite solar cell. *J. Electr. Mater.* 52, 7842 (2023).

2. Y. Li, D. Liang, X. Zhang, Z. Xiong, B. Tang, F. Si, Z. Fang, H. Li, Z. Shi, and J. Chen, Crystal structure, sintering behavior, and microwave dielectric properties of low-permittivity Ba₂Zr₂Si₃O₁₂ ceramics. *J. Electron. Mater.* 52, 7164–7170 (2023).

3. T. Fazal, S. Iqbal, M. Shah, A. Bahadur, B. Ismail, H.S.M. Abd-Rabboh, R. Hameed, Q. Mahmood, A. Ibrar, M.S. Nasar, Y. Ehsan, A.N. Shah Saqib, and M.A. Qayyum. Adnan, Deposition of bismuth sulfide and aluminum doped bismuth sulfide thin films for photovoltaic applications. *J. Mater. Sci. Mater. Electron.* 33, 42–53 (2022).

4. T. Fazal, S. Iqbal, M. Shah, Q. Mahmood, B. Ismail, H.O. Alsaab, N.S. Awwad, H.A. Ibrahium, and E.B. Elkaeed, Optoelectronic, structural and morphological analysis of Cu₃BiS₃ sulfosalt thin films. *Results Phys.* 36, 105453 (2022).

5. A. Rana, Lalita, S.P. Khanna, R. Srivastava, and C.K. Suman, Investigation of structural, optical, and photo-response properties of photochemical UV assisted CBD-grown CdS thin films. *J. Electron. Mater.* 52, 7302–7314 (2023).

6. T. Fazal, S. Iqbal, M. Shah, B. Ismail, N. Shaheen, H. Alrbyawi, M.M. Al-Anazy, E.B. Elkaeed, H.H. Somaily, R.A. Pashameah, E. Alzahrani, and A.-E. Farouk, Improvement in optoelectronic properties of bismuth sulphide thin films by chromium incorporation at the orthorhombic crystal lattice for photovoltaic applications. *Molecules* 27, 6419 (2022).

7. R.I. Daniel, R. Govindaraj, P. Ramasamy, and A.K. Chauhan, Enhancement of hole extraction in carbon-based organic-inorganic hybrid perovskite solar cells using MAPbI₃:NiO-NPs composite. *J. Electron. Mater.* 52, 7459–7474 (2023).

8. T. Fazal, S. Iqbal, M. Shah, B. Ismail, N. Shaheen, A.I. Alharthi, N.S. Awwad, and H.A. Ibrahium, Correlation between structural, morphological and optical properties of Bi₂S₃ thin films deposited by various aqueous and non-aqueous chemical bath deposition methods. *Results Phys.* 40, 105817 (2022).

9. F. Xie, D. Mei, L. Qiu, Z. Su, L. Chen, Y. Liu, and P. Du, High-efficiency fiber-shaped perovskite solar cells with TiO₂/SnO₂ double-electron transport layer materials. *J. Electron. Mater.* 52, 4626–4633 (2023).

10. J. Younus, W. Shahzad, B. Ismail, T. Fazal, M. Shah, S. Iqbal, A.H. Jawhari, N.S. Awwad, and H.A. Ibrahium, Engineering the optical properties of nickel sulphide thin films by zinc integration for photovoltaic applications. *RSC Adv.* 13, 27415–27422 (2023).

11. M. Fida, S. Iqbal, M. Shah, T. Fazal, B. Ismail, H.U. Rehman, F.F. Al-Fawzan, E.B. Elkaeed, R.A. Pashameah, E. Alzahrani, and A.-E. Farouk, Mn²⁺ doped cobalt oxide and its composite with carbon nanotubes for adsorption-assisted photocatalytic applications. *Sustainability* 14, 16932 (2022).

12. X. Shao, Y. Shi, H. Wang, X. Sun, L. Yang, X. Li, and M. Wang, A review on advances in the gas-sensitive properties of perovskite materials. *J. Electron. Mater.* 52, 5795–5809 (2023).

13. M. Vijatović, J. Bobić, and B.D. Stojanović, History and challenges of barium titanate: Part II. *Sci. Sinter.* 40, 235–244 (2008).

14. M. Boulos, S. Guillemet-Fritsch, F. Mathieu, B. Durand, T. Lebey, and V. Bley, Hydrothermal synthesis of nanosized BaTiO₃ powders and dielectric properties of corresponding ceramics. *Solid State Ionics* 176, 1301–1309 (2005).

15. A.T. Barrows, A.J. Pearson, C.K. Kwak, A.D. Dunbar, A.R. Buckley, and D.G. Lidzey, Efficient planar heterojunction mixed-halide perovskite solar cells deposited via spray-deposition. *Energy Environ. Sci.* 7(9), 2944–2950 (2014).

16. S. Niu, J. Milam-Guerrero, Y. Zhou, K. Ye, B. Zhao, B.C. Melot, and J. Ravichandran, Thermal stability study of transition metal perovskite sulfides. *J. Mater. Res.* 33, 4135–4143 (2018).

17. Z. Chen, J. Hu, Z. Lu, and X. He, Low-temperature preparation of lanthanum-doped BiFeO₃ crystallites by a sol–gel-hydrothermal method. *Ceram. Int.* 37, 2359–2364 (2011).

18. F. Guo, W. He, S. Qiu, C. Wang, X. Liu, K. Forberich, C.J. Brabec, and Y. Mai, Sequential deposition of high-quality photovoltaic perovskite layers via scalable printing methods. *Adv. Func. Mater.* 29, 1900964 (2019).

19. S. Abel, F. Eltes, J.E. Ortmann, A. Messner, P. Castera, T. Wagner, D. Urbonas, A. Rosa, A.M. Gutierrez, and D. Tulli, Large Pockels effect in micro-and nanostructured barium titanate integrated on silicon. *Nat. Mater.* 18, 42–47 (2019).

20. N. Labchir, E. Amaterz, A. Hannour, A. Ait Hssi, D. Vincent, A. Ihlal, and M. Sajieddine, Highly efficient nanostructured $CoFe_2O_4$ thin film electrodes for electrochemical degradation of rhodamine B. *Water Environ. Res.* 92, 759–765 (2020).

21. F.R. Estrada, L.G. de Moraes, F.L. Vital, M.D. Neme, P. Schio, T.J. Mori, and J.C. Cezar, Island growth mode in pulsed laser deposited ferroelectric BaTiO3 thin films: the role of oxygen pressure during deposition. *Ferroelectrics* 545, 39–44 (2019).

22. J.B. Whitaker, D.H. Kim, B.W. Larson, F. Zhang, J.J. Berry, M.F. Van Hest, and K. Zhu, Scalable slot-die coating of high performance perovskite solar cells. *Sustain. Energy Fuels* 2(11), 2442–2449 (2018).

23. B. Liu, M. Long, M. Cai, L. Ding, and J. Yang, Interfacial charge behavior modulation in 2D/3D perovskite heterostructure for potential high-performance solar cells. *Nano Energy* 59, 715–720 (2019).

24. Y. Wang, J. Yan, H. Cheng, N. Chen, P. Yan, F. Yang, and J. Ouyang, Lead zirconate titanate and barium titanate bi-layer ferroelectric films on Si. *Ceram. Int.* 45, 9032–9037 (2019).

25. N. Bouaniza, N. Hosni, and H. Maghraoui-Meherzi, Structural and optical properties of Cu_3SbS_3 thin film deposited by chemical bath deposition along with the degradation of methylene blue. *Surf. Coat. Technol.* 333, 195–200 (2018).

26. E. Yücel, N. Güler, and Y. Yücel, Optimization of deposition conditions of CdS thin films using response surface methodology. *J. Alloy. Compd.* 589, 207–212 (2014).

27. J. Britt and C. Ferekides, Thin-film CdS/CdTe solar cell with 15.8% efficiency. *Appl. Phys. Lett.* 62, 2851–2852 (1993).

28. J. Han, C. Spanheimer, G. Haindl, G. Fu, V. Krishnakumar, J. Schaffner, C. Fan, K. Zhao, A. Klein, and W. Jaegermann, Optimized chemical bath deposited CdS layers for the improvement of CdTe solar cells. *Sol. Energy Mater. Sol. Cells* 95, 816–820 (2011).

29. M. Zahid, N. Nadeem, M.A. Hanif, I.A. Bhatti, H.N. Bhatti, and G. Mustafa, *Metal Ferrites and Their Graphene-Based Nanocomposites: Synthesis, Characterization, and Applications in Wastewater Treatment, Magnetic Nanostructures* (Berlin: Springer, 2019), pp.181–212.

30. S. Khan, N. Humera, S. Niaz, S. Riaz, S. Atiq, and S. Naseem, Simultaneous normal—anomalous dielectric dispersion and room temperature ferroelectricity in CBD perovskite $BaTiO_3$ thin films. *J. Market. Res.* 9, 11439–11452 (2020).

31. L. Bakueva, I. Gorelikov, S. Musikhin, X.S. Zhao, E.H. Sargent, and E. Kumacheva, PbS quantum dots with stable efficient luminescence in the near-IR spectral range. *Adv. Mater.* 16, 926–929 (2004).

32. A. Ubale, Effect of complexing agent on growth process and properties of nanostructured Bi_2S_3 thin films deposited by chemical bath deposition method. *Mater. Chem. Phys.* 121, 555–560 (2010).

33. A. Kojima, K. Teshima, Y. Shirai, and T. Miyasaka, Organometal halide perovskites as visible-light sensitizers for photovoltaic cells. *J. Am. Chem. Soc.* 131, 6050–6051 (2009).

34. T. Baikie, Y. Fang, J.M. Kadro, M. Schreyer, F. Wei, S.G. Mhaisalkar, M. Graetzel, and T.J. White, Synthesis and crystal chemistry of the hybrid perovskite ($CH_3 NH_3$) PbI_3 for solid-state sensitised solar cell applications. *J. Mater. Chem. A* 1, 5628–5641 (2013).

35. J. Sun and D.J. Singh, Electronic properties, screening, and efficient carrier transport in $NaSbS_2$. *Phys. Rev. Appl.* 7, 024015 (2017).

36. S. De Wolf, J. Holovsky, S.J. Moon, P. Loper, B. Niesen, M. Ledinsky, F.J. Haug, J.H. Yum, and C. Ballif, Organometallic halide perovskites: sharp optical absorption edge and its relation to photovoltaic performance. *J. Phys. Chem. Lett.* 5(6), 1035–1039 (2014).

37. E. Yücel and Y. Yücel, Optimization of zinc sulfide thin film coating process using response surface methodology. *J. Mater. Sci.: Mater. Electron.* 26, 196–203 (2015).

38. S. Chu, and A. Majumdar, Opportunities and challenges for a sustainable energy future. *Nature* 488, 294–303 (2012).

39. P.-J. Alet, S. Palacin, P.R.I. Cabarrocas, B. Kalache, M. Firon, and R. De Bettignies, Hybrid solar cells based on thin-film silicon and P3HT: A first step towards nano-structured devices. *Eur. Phys. J. Appl. Phys.* 36, 231–234 (2006).

40. A. Khaleghi, S.M. Sadrameli, and M. Manteghian, Thermodynamic and kinetics investigation of homogeneous and heterogeneous nucleation. *Rev. Inorg. Chem.* 40, 167–192 (2020).

41. M.J. Bradshaw, Global energy dilemmas: a geographical perspective. *Geogr. J.* 176, 275–290 (2010).

42. H.H. Ahmed, Variation of the structural, optical and electrical properties of CBD CdO with processing temperature. *Mater. Sci. Semicond. Process.* 66, 215–222 (2017).

43. M.M. Gomaa, G.R. Yazdi, S. Schmidt, M. Boshta, V. Khranovskyy, F. Eriksson, B.S. Farag, M.B.S. Osman, and R. Yakimova, Effect of precursor solutions on the structural and optical properties of sprayed NiO thin films. *Mater. Sci. Semicond. Process.* 64, 32–38 (2017).

44. S.H. Chaki, M.P. Deshpande, J.P. Tailor, M.D. Chaudhary, and K.S. Mahato, Study of surface microstructure and optical properties of as-grown Mo0.6W0.4Se2 single crystals. *AIP Conf. Proc.* 1512, 882–883 (2013).